Mathematical Biosciences and Engineering

MBE, 18(2): 1898–1925.
DOI: 10.3934/mbe.2021099
Received: 13 December 2020
Accepted: 08 February 2021
Published: 22 February 2021

http://www.aimspress.com/journal/MBE

Research article

Defect reconstruction from magnetic flux leakage measurements employing modified cuckoo search algorithm

Daqian Zhang[1], Chen Huang[2,3,4,*] and Jiyou Fei[4]

[1] College of Aerospace Engineering, Shenyang Aerospace University, Shenyang 110136, China
[2] College of Civil Aviation, Shenyang Aerospace University, Shenyang 110136, China
[3] Shenyang Academy of Instrumentation Science, Shenyang 110043, China
[4] College of Mechanical Engineering, Dalian Jiaotong University, Dalian 116028, China

* **Correspondence:** Email: huangchen054@163.com.

Abstract: Accurate and efficient estimation for defect profile of magnetic flux leakage (MFL) signals is important for nondestructive evaluation in industry. To improve the accuracy of defect profile reconstruction, an improved reconstruction method based on modified cuckoo search (CS), called MCS, is proposed in this paper. Firstly, a novel single-dimension updating evolution strategy is proposed to avoid the interference between multiple dimensions, which can make full use of the appropriate nest position in the historical search. Secondly, an adaptive multi-strategy difference evolution is introduced into the evolution process to improve the diversity and efficiency of CS algorithm. The proportion factor of each strategy in multi-strategy difference evolution is adjusted dynamically according to the value of the objective fitness. Finally, various MFL signals are selected to verify the effectiveness of the proposed MCS algorithm. The experiment results illustrate that the proposed method has high performance on the quality of the solution and robustness for noise.

Keywords: defect profile reconstruction; cuckoo search; single-dimension; multi-strategy difference evolution; MFL signals

1. Introduction

For the nondestructive testing problem, the solution methods can be classified into three different categories: magnetic flux leakage (MFL) testing [1,2], eddy current testing [3,4], and ultrasonic testing [5]. Among these methods, the MFL technique is a highly efficient and popular

method of nondestructive testing (NDT) [6], which has been widely applied in pipeline nondestructive due to many advantages, such as high reliability, fast scanning and digital signal processing [7,8]. Early detection of the pipe faults according to the result of magnetic flux leakage (MFL) inspection may avoid severe collapses that involve environmental damage and high costs. Reconstructing defect profiles from MFL measurements is a typical inverse problem in MFL testing. An efficient solution for an inverse problem to estimate the defects from MFL signals is very important to enhance the accuracy of defect measurement [9,10]. The defect dimension of the pipelines determines whether the severity and repair urgency of defects need to be established.

The direct method to estimate the defect inversing is to obtain the geometry parameters of the defects in early studies, such as the equivalent length, width, and depth. Although the method is simple and fast, the accuracy of the reconstruction is low and the defect of arbitrary shape can not be reconstructed. Then, in order to meet the requirement for higher precision, the actual profile of the defect is accurately reconstructed by an iterative inversion method. For this method, the defect contour reconstruction can be considered as an optimization problem to solve by minimizing the difference between the reference signal and the predicted signal iteratively. The iterative inversion method has two essential components: the forward model and the update strategy of defect profile.

The forward model is used to predict the magnetic response of ferromagnetic materials. There are several models for the forward model, e.g., analytical model, numerical model and heuristic model. Magnetic dipole model, as a typical analytical model, is not suitable to calculate the complex defect. In order to overcome the drawback of the magnetic dipole model, the finite-element method (FEM) [11,12], which belongs to numerical model, is used to calculate the distribution of magnetic leakage field. Compared with the analytical model of magnetic dipole model, FEM can exploit different shapes and sizes units to approximate the distribution of leakage magnetic field in the different defect position with irregular profiles, but unfortunately the computational expense will be very expensive. Heuristic model is mainly based on the application of various machine learning methods. Artificial neural network (ANN), e.g., RBFNN [13,14], as the most commonly used heuristic model method, can be trained by a lot of prior defect profile and the corresponding MFL signal, then approximate highly nonlinear functions efficiently. The calculation speed of heuristic model is obviously faster than other methods.

As the core of the iterative inversion method, the updating process of the defect profile aims to provide the high quality candidate predict profiles. Many optimization algorithms have been applied to update the defect profile in the inversing process. Priewald et al. [11] presented a fast and effective algorithm for reconstructing arbitrary defect profiles based on a nonlinear FEM forward model and a rapidly converging Gauss-Newton optimization to update the defect model. Hari et al. [13] adopted genetic algorithm (GA) as the optimization technique to determine the shape, the size and the place of defect considering the nonlinearity of the pipe material. Li et al. [15] proposed to employ a modified harmony search (MHS) algorithm with a multiple selection opposition-based learning strategy to update the defect profile. Zhang et al. [16] proposed particle swarm optimization algorithm (PSO) to reconstruct the sizes of rectangular crack.

So far intelligent algorithms have attracted more and more attention [17–19], particle swarm optimization (PSO) [20], difference evolution (DE) [21], ant colony optimization (ACO) [22], genetic algorithm (GA) etc. Cuckoo search (CS) algorithm [23,24] is a new intelligent optimization algorithm, which is presented under the inspiration of cuckoo breeding behavior with levy flight. CS algorithm has many advantages, which include few parameters, simple operation, easy

implementation, strong ability of searching and so on. The CS algorithm is widely used in solving with optimal problems, such as function optimization, power system optimization and parameter estimation. In the study and application of the CS algorithm, it is found that the CS algorithm [25,26] has some drawbacks of weak local search ability, slow convergence speed and easy to get into the local solution. Therefore, in order to solve these shortcomings, a modified CS (MCS) algorithm based on single dimensional evolution strategy and multi-strategy difference evolution are introduced in original CS algorithm.

The innovations and main contributions of this paper are described as follows.

•An improved reconstruction method based on modified cuckoo search (CS), called MCS, is proposed to improve the accuracy of defect profile reconstruction.

•The single dimensional evolution is firstly proposed to optimize the process of the evolution. The dimension with the maximum error between preference signals and predicted signals is selected to update the position of its nest in CS algorithm.

•The DE with multi-strategy evolution is complemented to optimize the initial CS algorithm by the way of increasing the diversity of the swarm. The multi-strategy evolution can avoid the species into the local optimum, consequently the algorithm ability of global optimization is enhanced.

The remainder of the paper is organized as follows. The principle of the defect reconstruction problem is described in Section 2. The traditional CS algorithm is presented in Section 3. The modified CS algorithm is introduced in Section 4. The modified CS algorithm is used to estimate the defect profile in Section 5. The experimental results to demonstrate the performance of the proposed method are given in detail in Section 6. Finally, Section 7 concludes this paper and discusses future research direction.

2. Forward model of MFL signals

Ferromagnetic materials are magnetized under the action of external magnetic field, which leads to leakage magnetic field at defects. Due to the high magnetic permeability of ferromagnetic materials, the magnetic induction field of magnetized materials is relatively strong. When the materials are defective, the non-continuity of material properties leads to the magnetic refraction at the interface where they contact with the air, and the magnetic induction field in ferromagnetic materials is deflected to the air, forming magnetic diffusion.

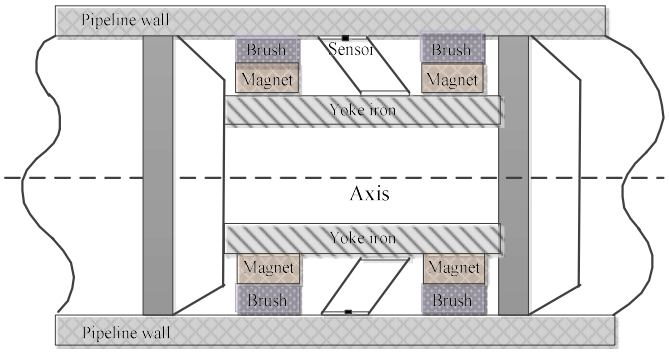

Figure 1. The physical model of the MFL inspection system.

The principle of three-axis magnetic flux leakage detection is to saturate and magnetize the tube wall with permanent magnet, so that the tube wall between magnetic iron reaches the state of magnetic saturation, and then transfers to another steel brush and permanent magnet. The two permanent magnets are connected by yoke iron, and the permanent magnet steel brush tube wall and iron core finally form a magnetic circuit. The complete physical model of the MFL inspection system is shown in Figure 1, which mainly consists of permanent magnet, steel brushes, yoke iron, sensor and the inspected pipe wall.

The solid model is built according to the working state of the detection equipment in the pipeline with MFL. Since the detection model of the pipeline is axisymmetric, this model is built by selecting the radial profile of the detection equipment in the pipeline with MFL. The axial simplified model of the MFL inspection system is depicted in Figure 2.

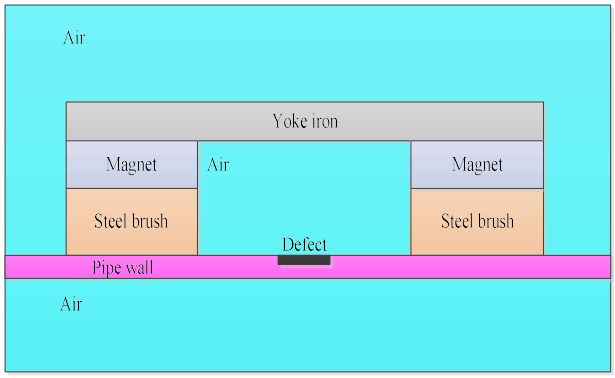

Figure 2. The axial simplified model of FEM.

X52 steel is chosen as the material of the pipeline wall, its B-H curve is described in Figure 3. When the magnetic force line passes through the pipe wall, the magnetic force line passes through the pipe wall without defects and is evenly distributed. As shown in Figure 4. When there are defects in the pipe wall, the cross-sectional area of the pipe wall where the defects become smaller. As the permeability of the pipeline wall at the defects is far less than that of the pipe wall, the magnetic path at the defects becomes smaller and the magneto-resistance becomes larger. Finally, the magnetic force line is distorted, and a leakage magnetic field is formed when the pipe wall at the defects penetrates through the pipe wall. Figures 5 and 6 show the MFL signal corresponding to a group of rectangular defects with the same length and different depths. Figure 5 describes the axial component of the MFL signal, and Figure 6 shows the radial component.

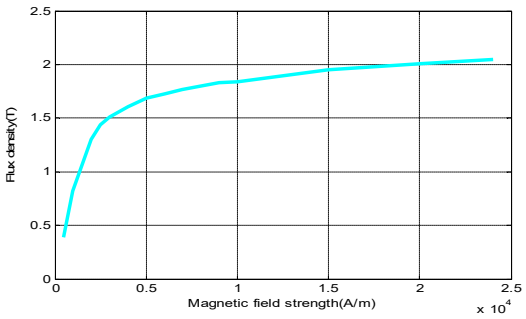

Figure 3. The B-H curve of X52 steel.

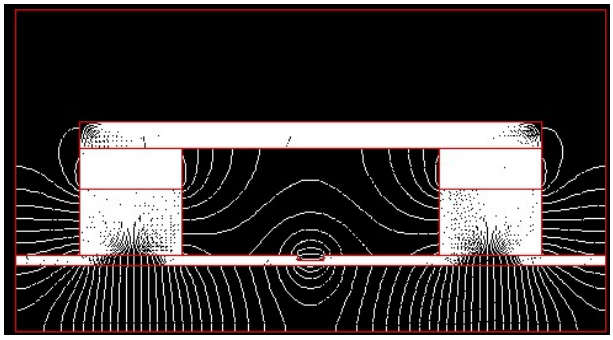

Figure 4. Distribution of magnetic flux density with defect.

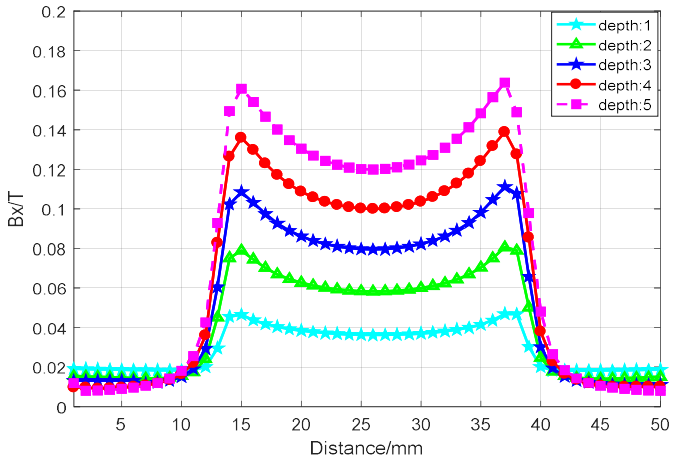

Figure 5. Axial components of MFL signals for a series of defects with the same length and different depths.

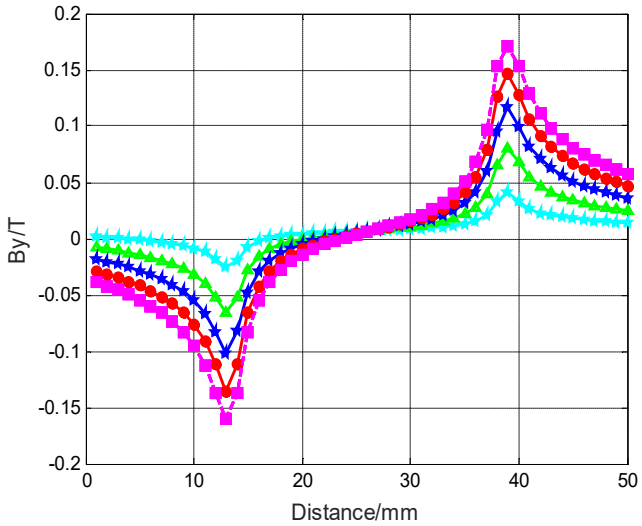

Figure 6. Radial components of MFL signals for a series of defects with the same length and different depths.

FEM is adopted as the forward model to generate MFL signal, which provides a large number of samples for Radial-basis function neural network (RBFNN) to train. RBFNN utilizes a fast learning

speed and learning convergence speed to approximate the forward model. In RBFNN frame, there is three-layer neural network, including input layer, hidden layer and output layer. The size of the samples is proportional to the increased training accuracy.

The data extracted from the defects of pipeline wall is used as the input vector, and the MFL signal of different defects is regarded as the target output vector for the common defects. A highly uncertain nonlinear system can be achieved through the network operation. The model can be expressed mathematically as

$$y_i = \sum_{j=1}^{M} w_{ij} \cdot \phi(\|x - c_j\|) \tag{1}$$

where y_i is the *i*-th output component of the radial basis function, w_{ij} is the weight value of the input vector in the network, c_j is the center of the *i*-th radial basis function, and *M* is the total number of radial basis functions.

The Gauss function is the most commonly used radial basis function, so it is denoted as

$$\phi(\|x - c_j\|) = \exp(-\frac{\|x - c_j\|^2}{2\sigma_j^2}) \tag{2}$$

where σ_j is the standard deviation of the Gauss function. Substitute Eq (2) into Eq (1), the relation between input and output of the neural network with the Gauss function as the radial basis function can be written as

$$y_i = \sum_{j=1}^{M} w_{ij} \cdot \exp(-\frac{\|x - c_j\|^2}{2\sigma_j^2}) \tag{3}$$

3. Cuckoo search algorithm

Cuckoo search algorithm is a new and effective population-based optimization algorithm to solve high-dimension optimization problems. The algorithm is designed by the observations on the breeding behavior of cuckoo birds. It is called that certain species of cuckoos select suitable birds' nests to lay their eggs with the Lévy flights behavior [25–27]. Once the host bird discovers the presence of the cuckoo's eggs, the host bird will discard the cuckoo's eggs or rebuilds a new nest. In Cuckoo algorithm, Lévy flights random walks is utilized to replace isotropic random walks in GA and PSO algorithms. So it is more efficient than many swarm-based intelligent optimal algorithms. Its step is a random walk that satisfies a stable distribution of a heavy tail. CS has the three assumptions as follows.

(I) Each cuckoo lays only one egg at a time, and its egg is randomly put into a nest;

(II) The nests with the highest quality of eggs will carry over to the next generation;

(III) The number of host's nests is fixed, and the cuckoo egg is discovered by the host with the probability $P_a \in [0,1]$.

For the actual optimization problem, it is noted that a candidate solution in the search space is equivalent to the position of a nest with *D* dimension. On the basis of current solution, there are two important operations to update the solution. The first one is the nest position of the next generation is generated through Lévy flight. The position $x_k^d(t+1)$ of the new nest by Lévy flight is updated

according to the following equation

$$x_k^d(t+1)=x_k^d(t)+c_1\frac{\phi\times u}{|v|^{1/\beta}}(x_k^d(t)-gbnest^d) \tag{4}$$

with

$$\phi=\left(\frac{\Gamma(1+\beta)\times\sin(\pi\times\beta/2)}{\Gamma\left(\left(\frac{1+\beta}{2}\right)\times\beta\times2^{(\beta-1)/2}\right)}\right)^{1/\beta} \tag{5}$$

where $x_k^d(t)$ is the position of the d-th dimension for the k-th nest at t iteration; c_1 is a step length scaling factor. In general, c_1=0.01, and $gbnest^d$ is the d-th dimension of the best nest.

In Eq (11), $\frac{u}{|v|^{1/\beta}}$ is the step size obeying a given Lévy distribution.

Where β is a constant, both u and v follow a normal distribution

$$\begin{cases} u\sim N(0,\sigma_u^2) \\ v\sim N(0,\sigma_v^2) \end{cases} \tag{6}$$

After new nest is obtained by Lévy flight, it is possible that cuckoo egg in a host nest is found by its host bird with the probability P_a. Random migration is the second important operation to update the solution. Random migration will produce a new solution to replace the previous one by two different solutions randomly selected from current solutions, and the updated formula is

$$x_k^d(t+1)=x_k^d(t)+r\left(x_i^d(t)-x_j^d(\mathrm{t})\right) \tag{7}$$

where r is a random number over the range [0, 1]. $x_i^d(t)$ and $x_j^d(t)$ are two different nest position randomly selected from current nest at t iteration, respectively.

The new generated solution may be out of the search space, so the solution should be constrained as follows

$$x_k^d(t+1)=\begin{cases} x_k^d(t+1) & if\ \ x_{\min}^d<x_k^d(t+1)<x_{\max}^d \\ x_{\min}^d & if\ \ x_k^d(t+1)<x_{\min}^d \\ x_{\max}^d & if\ \ x_k^d(t+1)>x_{\max}^d \end{cases} \tag{8}$$

where $x_{\min}^d$ and $x_{\max}^d$ are the lower and upper range of the d-th dimension of the k-th solution, respectively.

4. Modified cuckoo search algorithm

Although cuckoo search algorithm has many advantages, e.g. strong global optimization ability and few parameters, it still has some drawbacks, such as low convergence speed, poor population diversity etc. Specifically, the major improvement of MCS algorithm includes the following two aspects.

4.1. Single dimension evolution

In CS algorithm, each nest is updated and evaluated as a whole to investigate the effectiveness of algorithm evolution. It means that each dimension in each nest location will be updated, and all new generated dimensions will be evaluated as a whole. This overall updated and evaluation strategy is effective for single-dimensional optimization problems. However, for multi-dimensional problems, the search speed and convergence accuracy of the algorithm will be restricted due to the coupling phenomenon between multi-dimensions. The traditional CS algorithm does not make full use of the information of the current candidate solution. Therefore, the single dimension evolution strategy is adopted to optimize the quality of obtained solution to improve the search efficiency of CS algorithm.

Each generation of single evolution strategy only updates the solution of single dimension. In view of the correspondence between the defect signal and the corresponding MFL signal, the single evolution dimension is selected according to the difference between the reference signal and the MFL single of the estimated global best defect profile at current iteration. The selection of the dimension can be derived from the following equation

$$d_0^t = \arg\max_i (RP_i - \widehat{PP}_{gi}^t) \tag{9}$$

$$d^t = N(d_0^t, s) \tag{10}$$

where RP_i is the *i*-th component of the reference signal, $\widehat{PP}_{gi}$ is the *i*-th dimension of the global best nest at *t* iteration. $N(d_0, sigma)$ is Gaussian distribution with mean d_0 and standard deviation s.

The *i*-th dimension is updated according to Eq (4), the obtained new dimension together with the other dimensions constitutes a new candidate solution, and it is appraised by the objective function value. If the value is better than the function fitness value of the last generation, keep the candidate solution and continue to evolve until meet the stop condition. Due to the adoption of the greed rule, the algorithm only accepts new values that can improve the current candidate solutions, which ensures the target tuning of the search direction during the optimization process of the algorithm and does not affect the efficiency of the algorithm. Due to the single-evolution evaluation strategy using the greed rule, it will not abandon the global optimal evolution direction because of the degeneration of some dimensions. The single-dimension information guidance is used to carry out effective search and obtain higher quality solution results.

4.2. Multi-strategy DE mutation

In the cuckoo search algorithm, firstly the random search by Lévy Flight is designed to obtain new solutions, and then the part of the obtained nests are discarded to rebuilt new nest according to the probability P_a. The second important process is designed on the basis of randomly selected nests from the population, to generate new nest position solution. In order to improve the population diversity, multi-strategy difference evolution is introduced into CS algorithm. A new updating strategy is designed on the basis of three following kinds of difference evolution strategies.

As an important branch of evolutionary algorithm, difference evolution is a heuristic global random search algorithm based on the differences among individuals [28]. The individual of the difference evolution algorithm will generate new individuals through mutation operation. The commonly used mutation strategy [29] is summarized as

DE/Rand/2:

$$v_i(t) = x_{r1}(t) + F \cdot (x_{r2}(t) - x_{r3}(t)) + F(x_{r4}(t) - x_{r5}(t)) \tag{11}$$

DE/Best/1:

$$v_i(t) = x_{best}(t) + F \cdot (x_{r2}(t) - x_{r3}(t)) \tag{12}$$

DE/Best/2:

$$v_i(t) = x_{best}(t) + F \cdot (x_{r2}(t) - x_{r3}(t)) + F \cdot (x_{r4}(t) - x_{r5}(t)) \tag{13}$$

Current-to-best/1:

$$v_i(t) = x_i(t) + F \cdot (x_{best}(t) - x_i(t)) + F \cdot (x_{r1}(t) - x_{r2}(t)) \tag{14}$$

where F is the weighted factor; $r_1, r_2, r_3, r_4, r_5 \in [1, N]$ are random number; N is the number of the population; $x_{best}(t)$ is the best individual in the current group, *rand* is random number that obey uniform distribution of [0, 1].

MCS algorithm combines Eqs (11)–(14) as the new random migration strategy which is used to rebuilt the solutions which have been abandoned according to the proportion P_a. New random migration strategy consisting four choices can enhance the search efficiency and enrich the diversity of cuckoos. When a few of evolution strategies are implemented, we should consider the performance of each evolutionary strategy in each generation. The scaling factor is designed to be dynamically adjusted associated with the evaluation function. The MCS algorithm retains the global searching ability of CS algorithm, and improves local searching ability of CS algorithm. It provides an effective and feasible method to extract the characteristic of adaptive multi-strategy mutation process for DE algorithm.

4.3. Adaptive parameter strategy

The control parameters of MCS algorithm have an important influence on its optimization performance. Generally the control parameters are determined by traditional empirical methods which cannot always maintain the optimality.

The global search of MCS algorithm is carried out by adaptive Levy flight mechanism, the Levy flight step size decreases with the iteration. The improved algorithm has a larger step size factor in the initial stage of optimization, so as to expand the search space and improve the global search ability; in the process of optimization, the step size is reduced to improve the local search performance of the algorithm. The adaptive strategy of the step length scaling factor c_1 is described

$$c_1 = 0.001 \times T_{\max} \times \exp(-(T / T_{\max})) \tag{15}$$

The probability P_a of each generation is obtained by normal distribution, which can be expressed as

$$P_a^{t+1} = randn(M_P^{t+1}, 0.001) \tag{16}$$

In the evolution process, if the individual is better than that of the parent after multi strategy differential mutation, the corresponding P_a will be stored in S_F set. At the end of each generation

evolution, M_p is updated as follows

$$M_P^{t+1} = \begin{cases} mean(S_F), & \text{if } S_F \neq \phi \\ M_P^t, & \text{else} \end{cases} \tag{17}$$

According to the experience, the value of F should increase with the number of iterations. When the algorithm begins, F should be small, and in the later stages of the algorithm, the value of F will get large. Therefore, F is set as follows,

$$F = F_{\max} - T \cdot (F_{\max} - F_{\min}) / T_{\max} \tag{18}$$

Where $F_{\max}$ and $F_{\min}$ are the upper and lower bounds of F.

4.4. Complete optimization procedure of the MCS

The MCS algorithm with single dimension search and adaptive multi-strategy different evolution is described as follows in detail.

Step 1. Initialize the MCS algorithm.

Set the size of nests N, the maximum number of iterations $T_{\max}$, the upper and lower bounds of search space, step length scaling factor c_1 and the probability P_a. Randomly generate the positions of N nests.

Step 2. Calculate the fitness value.

Calculate the fitness value of each individual, and choose the best position of the individual and the global optimum as the current position of cuckoo nests and best individual.

Step 3. Select the dimension of evolution.

The dimension is selected according to Eqs (9) and (10).

Step 4. Update single dimension of the nests by Lévy flight.

The selected dimension is updated by using Lévy flight, which together with the others forms the new nests. The fitness of new nests is calculated according to the evaluation function, where the quality of new nests positions will be measured. If the fitness of the new nest positions is better than the old one, the previous nest can be replaced by the new nest.

Step 5. Abandon and construct the new single dimension of the nest position.

The corresponding selection boundaries of four policies are written as P_{a1}^t, P_{a2}^t, P_{a3}^t, P_{a4}^t at t generation. The current dimension is updated as

$$x_k^d(t+1) = \begin{cases} x_k^d(t) + r\left(x_i^d(t) - x_j^d(t)\right), 0 \le r \le P_{a1}^t; \\ x_{r1,g} + F \cdot (x_{r2,g} - x_{r3,g}), \ P_{a1}^t < r \le P_{a2}^t; \\ x_{r1,g} + F \cdot (x_{r2,g} - x_{r3,g}) + F \cdot (x_{r4,g} - x_{r5,g}), P_{a2}^t < r \le P_{a3}^t; \\ x_{i,g} + rand \cdot (x_{r1,g} - x_{i,g}) + F \cdot (x_{r2,g} - x_{r3,g}), \ P_{a3}^t < r \le P_{a4}^t. \end{cases} \tag{19}$$

with

$$\begin{cases} P_{a1}^t = 0.25 * P_a * k_1^t; \\ P_{a2}^t = P_{a1} + 0.25 * P_a * k_2^t; \\ P_{a3}^t = P_{a2} + 0.25 * P_a * k_3^t; \\ P_{a4}^t = P_{a3} + 0.25 * P_a * k_4^t; \end{cases} \tag{20}$$

According to 1/5 principle which is proposed by Rechenberg [30], the adjust rule of factor in strategy is calculated as

$$k_1^{t+1}=\begin{cases} k_1^t * f_k, a_1 > 0.3; \\ k_1^t,\ 0.2 \le a_1 < 0.3; \\ k_1^t / f_k,\ a_1 < 0.2. \end{cases} \quad \text{with} \quad a_1=\frac{n_1}{s_1} \tag{21}$$

where a_1 is the improvement rate of Eq (11); n_1 is the number the current solutions which are better than the previous ones; s_1 is the total number of the individuals which are used to update by the first strategy. The adjust rule of k_2^{t+1}, k_3^{t+1} and k_4^{t+1} are similar to k_1^{t+1}, when $t=0, k_1^0=k_2^0=k_3^0=k_4^0; f_k>1$.

In order to prevent the parameter be overturned, it is noted the upper and lower of f_k should be determined before the start of the run. If the dimension exceeds the search space, then it is limited into the boundary value of search space.

Step 6. Determine the end condition.

Determine whether the end conditions are met. If the end condition is met, the global optimum value and position of nest are recorded. Otherwise, turn to Step 2.

5. Inversing approach based on MCS

On the basis of the above section, MCS algorithm is used to reconstruct the defect profile. The flow chart of which is shown in Figure 7.

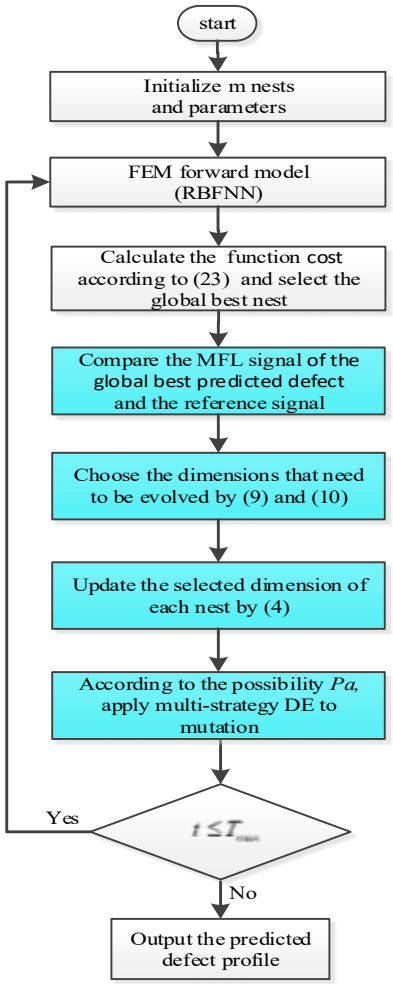

Figure 7. The flow of MCS-based algorithm.

The algorithm is implemented using the following steps in detail.

Step 1. Initialize the nests of the MCS algorithm and set all the parameters, e.g., the number of the nests *N*, the maximum iteration of $It_{\max}$, the probability P_a, and step length scaling factor c_1. *N* nests of MCS algorithm represent the predicted profiles as

$$\begin{bmatrix} PP_{11} & PP_{12} & \cdots & PP_{1D} \\ PP_{21} & PP_{22} & \cdots & PP_{2D} \\ \vdots & \vdots & \ddots & \vdots \\ PP_{N1} & PP_{N2} & \cdots & PP_{ND} \end{bmatrix} \tag{22}$$

Step 2. Compute the MFL signal of the corresponding nest by the RBFNN, the obtained data from the FEM forward model are used to train the RBFNN, which can be more accurate to approximate the relationship between profile signal and the MFL signal.

Step 3. Calculate the fitness value of each nest according to the given preference profile using the formula as

$$f(\widehat{PPx}_{ij}) = \sum_{j=1}^{D} (RBx_j - \widehat{PPx}_{ij})^2 \tag{23}$$

The best nest is selected by the fitness value *f*.

Step 4. Generate the new nests by MCS algorithm.

Step 5. Determine whether the maximum number of the iterations is met. If $t \le T_{\max}$, turn to Step 2. Otherwise, output the final predicted defect profile.

6. Performance evaluation

To test the performance of the proposed approach, some defects with different profiles were reconstructed in the experiment. The MFL data was generated from ANSYS 15.0 software. The defects with 360 samples were used to produce the corresponding MFL signals. Among the 360 defects, 240 profiles were rectangular defects, 80 profiles were ladder defects, and the remaining 40 profiles were triangular. The data were divided into two groups. The first group including 340 pairs was used for training by RBFNN and the second group was used to test the reconstruct result of the proposed inversing approach. The dimension number of defect profile was 50, so the number of input and output layers of RBFNN was also 50.

In order to evaluate the error between the true defect profile and reconstruction predicted profile, overall proximate degree PSD could be utilized as an important performance criterion. Besides that, the error PDE between the maximum depth of the true defect profile and the maximum depth of the predicted profile were taken account to estimate the severity of the defect. The PSD and PDE [15] are defined as follows,

$$PSD = \sqrt{\frac{1}{N_{DOF}} \sum_{i=1}^{N_{DOF}} (\mathrm{RP}_i - \mathrm{PP}_i)^2} \tag{24}$$

$$PDE = \left|\min(\mathrm{RP}) - \min(\mathrm{PP})\right| \tag{25}$$

The accuracy of defect assessment is mainly evaluated by the above two indicators. In practice, the actual MFL signals are often mixed by the normally distributed noise. The noise will affect the evaluated results, so we discussed the performance with the noise which had with an SNR of 20 dB.

All the simulation experiments were implemented on a PC with an Intel Core I7-9700 CPU and a 32 GB memory. For a reliable and fair comparison, all simulation experiments were ordered to execute 50 independent runs. The average results were calculated to demonstrate the performance of the different algorithms.

(I) Parameter setting

If there is no defect in the pipe, the depth of defect is defined as 0. In ANSYS model, pipe wall thickness was set to 8 mm. The scope of defect depth was from −8 to 1 mm, which constrained the search space for the solutions. So $X_{\min} = -8$ and $X_{\max} = 1$. In MCS algorithm, $P_a = 0.8$, $\beta = 1.5$, and $F = 0.8$, respectively. To show the effect of population size on the performance of the algorithm, we selected different population sizes from 50 to 500. Figures 8 and 9 display the simulation experimental results, including the results of the PSD and the PDE. The corresponding simulation experimental data is recorded in Table 1. The profiles and the MFL signal estimated by MCS are shown in Figure 10.

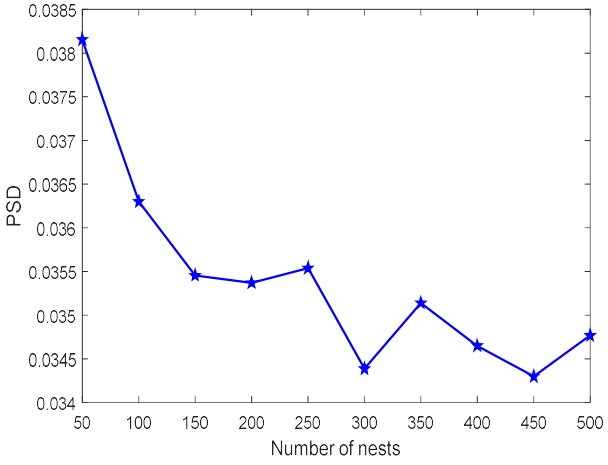

Figure 8. The result of the PSD.

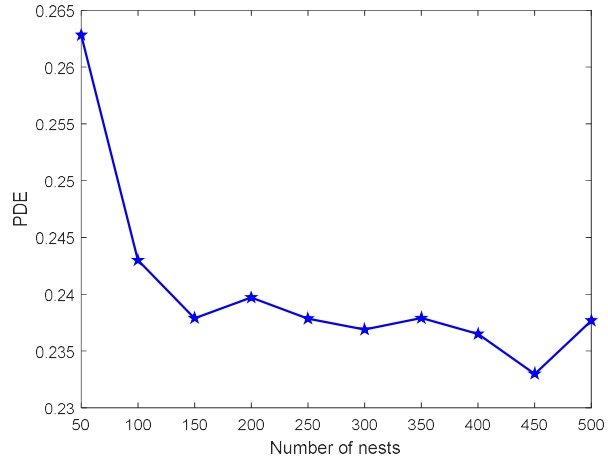

Figure 9. The result of the PDE.

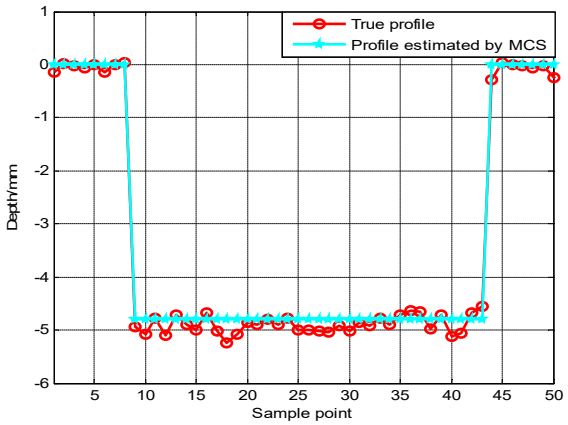

(a) The profiles estimated by MCS.

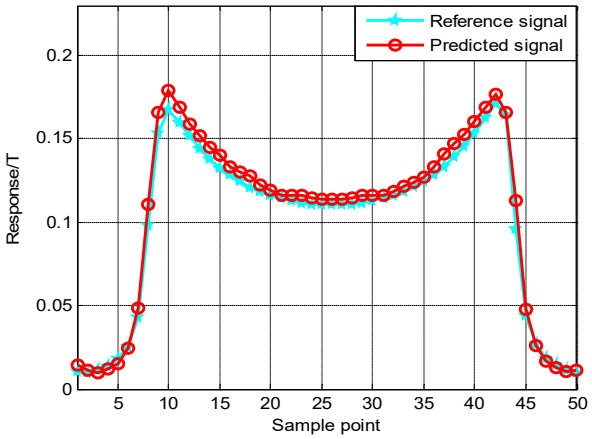

(b) The MFL signal estimated by MCS.

Figure 10. The profiles and the MFL signal estimated by MCS.

Table 1. The results of the PSD and the PDE.

Term	Number of nests				
	50	100	150	200	250
PSD	0.0382	0.0363	0.0355	0.0353	0.0354
PDE	0.2628	0.2431	0.2379	0.2398	0.2378
Term	Number of nests				
	300	350	400	450	500
PSD	0.0344	0.0351	0.0346	0.0343	0.0348
PDE	0.2369	0.2378	0.2365	0.2330	0.2377

From Figures 8 and 9, the results demonstrate that if the number of nests is too small, e.g., 50, the value of PSD and PDE is obviously larger than when N are other values. But when the number of nests was enough to predict the defect profile, e.g., 100, the number of nests had little influence on the change of the value of PSD and PDE.

(II) Performance comparison of different approaches without noise

To demonstrate the performance of the proposed algorithm, the nine defect profiles with different depth and width were adopted to reconstruct, which were randomly selected from the test set and presented in Table 2. The parameters in PSO, DE, CS, CS-PF [6] is given in Table 3. The results, including PSD and PDE, are listed in Table 4.

Table 2. The samples of nine defect profiles.

Sample index	Defects shape	Width (mm)	Depth (mm)
1	rectangle	10	1.6
2	rectangle	15	2.4
3	rectangle	25	3.2
4	triangle	41	4.4
5	triangle	45	5.6
6	triangle	35	3.6
7	trapezoid	34/15	2.0
8	trapezoid	8/3	5.6
9	trapezoid	21/9	7.2

Table 3. The parameters of five different algorithms.

Parameter	Value
Number of generations	100
Population size	100
Pa (CS, CS-PF, MCS)	0.8
β (CS, CS-PF, MCS)	1.5
T (CS-PF)	1
F (only DE)	0.7
CR (only DE)	0.8
w	0.73
c_1	1.5
c_2	1.5

Figures 11 and 12 and Table 4 show the reconstruction result of defect profile. It is noted that the best results among the five algorithms are indicated in bold. From Figures 11 and 12 and Table 4, it is obvious that MCS can achieve better result indicators, e.g., PSD and PDE, than the other approaches. PSD of CS-PF method was smaller than that of the other three methods (PSO, DE, CS) in most cases. It is clearly visible that MCS exceeds other algorithms significantly in three types of defect samples.

From the experiment, it could be concluded that the performance of MCS was better than the other four approaches. This results demonstrated that the proposed inversing approach based on MCS was effective and steady.

Table 4. Performance comparisons of five algorithms.

Sample index	Item	CS	CS-PF	DE	PSO	MCS
1	PSD	0.136	0.109	0.154	0.227	0.035
	PDE	0.975	0.517	1.067	0.903	0.202
2	PSD	0.130	0.122	0.142	0.218	0.050
	PDE	1.287	1.165	1.323	1.589	0.299
3	PSD	0.145	0.113	0.155	0.233	0.037
	PDE	1.295	0.806	1.351	1.607	0.260
4	PSD	0.142	0.135	0.173	0.262	0.061
	PDE	1.368	1.257	1.459	1.543	0.682
5	PSD	0.148	0.137	0.171	0.256	0.074
	PDE	1.435	1.245	1.477	1.526	0.870
6	PSD	0.137	0.133	0.178	0.249	0.057
	PDE	1.401	1.344	1.538	1.621	0.813
7	PSD	0.129	0.112	0.124	0.157	0.027
	PDE	1.319	1.231	1.406	1.453	0.216
8	PSD	0.117	0.106	0.122	0.186	0.059
	PDE	1.266	1.192	1.435	1.594	0.647
9	PSD	0.125	0.107	0.136	0.191	0.055
	PDE	0.800	1.238	1.474	1.614	0.292

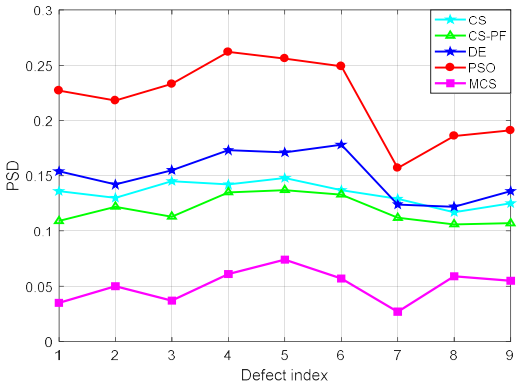

Figure 11. The PSD values of nine defect profiles without noise.

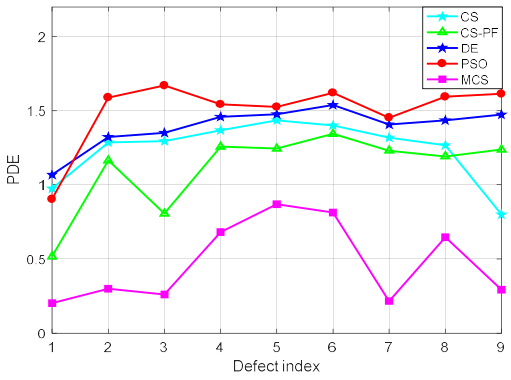

Figure 12. The PDE values of nine defect profiles without noise.

In the actual environment, noise signals are often included in the collected MFL measurement signals, so the performance of the reconstruction algorithm with noise added should be considered when the defect reconstruction is employed. To verify the performance of MCS about the robustness of the noise, the noise with an SNR of 20 dB was added to the above nine signals. The performances of the five different methods are described in Figures 13 and 14 and Table 5. Figures 15–23 display the reconstruction results of the defect profiles based on MCS. In these figures, the true profile is expressed by the blue line, and the predicted defect profile is represented by the red line.

Table 5. Performance comparisons of five algorithms with SNR of 20.

Sample index	Item	CS	CS-PF	DE	PSO	MCS
1	PSD	0.145	0.113	0.164	0.271	0.039
	PDE	1.063	0.628	1.362	1.217	0.230
2	PSD	0.168	0.127	0.176	0.286	0.053
	PDE	1.359	1.203	1.694	1.628	0.357
3	PSD	0.162	0.116	0.196	0.279	0.044
	PDE	1.534	0.885	1.479	1.716	0.287
4	PSD	0.270	0.169	0.211	0.337	0.069
	PDE	1.425	1.259	1.553	1.689	0.682
5	PSD	0.217	0.189	0.178	0.223	0.075
	PDE	1.493	1.305	1.637	1.787	0.870
6	PSD	0.148	0.121	0.197	0.226	0.056
	PDE	1.441	1.376	1.638	1.755	0.813
7	PSD	0.150	0.147	0.199	0.186	0.037
	PDE	1.513	1.320	1.607	1.516	0.216
8	PSD	0.139	0.115	0.242	0.196	0.062
	PDE	1.365	1.292	1.694	1.769	0.647
9	PSD	0.163	0.125	0.163	0.211	0.060
	PDE	0.820	0.702	1.165	1.518	0.292

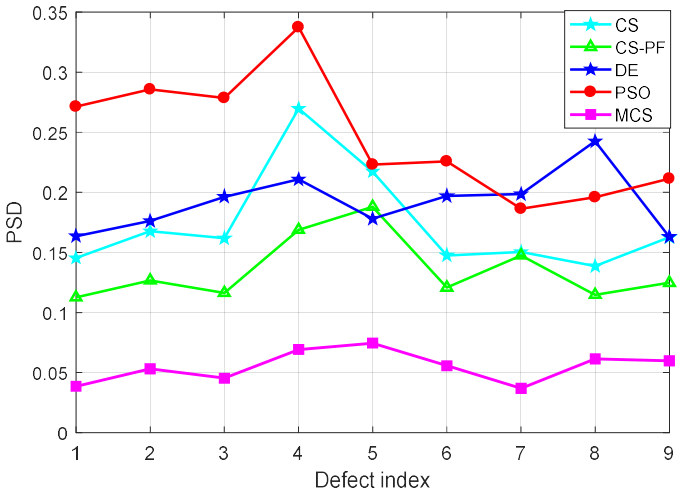

Figure 13. The PSD values of five different algorithms with noise.

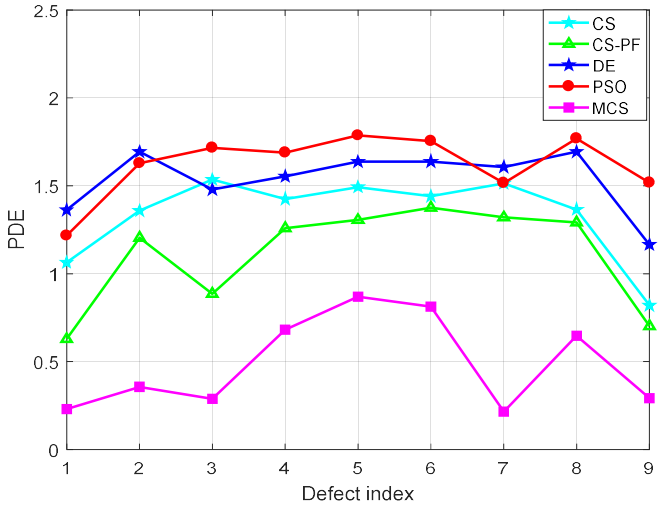

Figure 14. The PDE values of five different algorithms with noise.

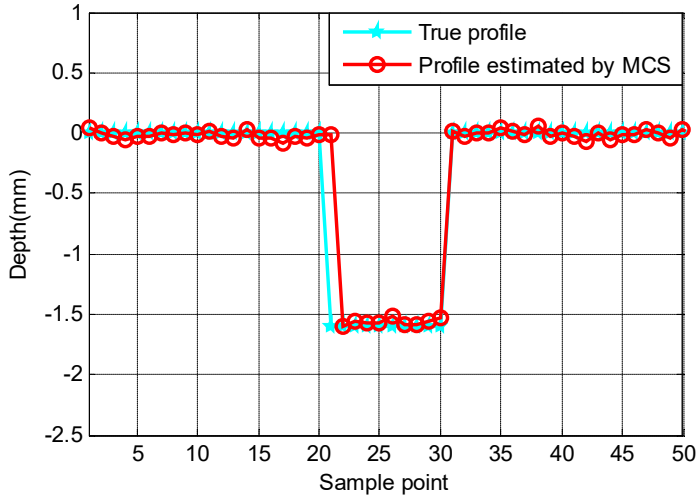

(a) The estimated defect profile of MCS algorithm.

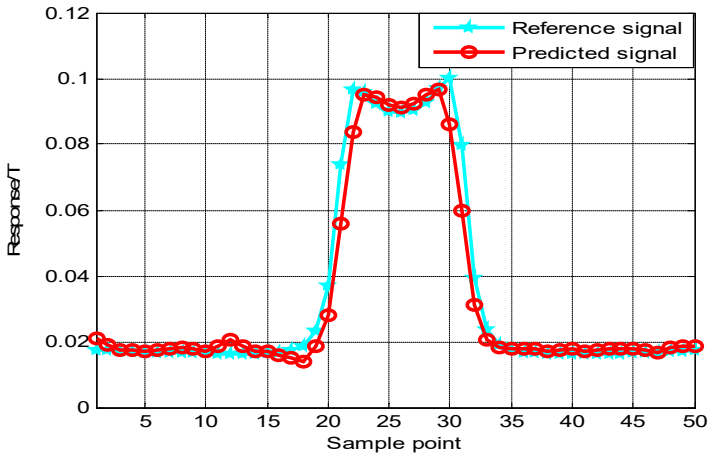

(b) The MFL single of MCS algorithm.

Figure 15. The result of MCS algorithm (sample No. 1).

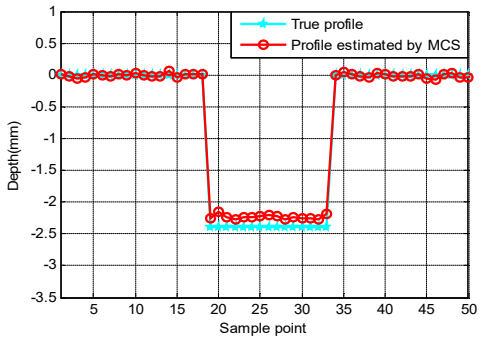

(a) The estimated defect profiles of MCS algorithm.

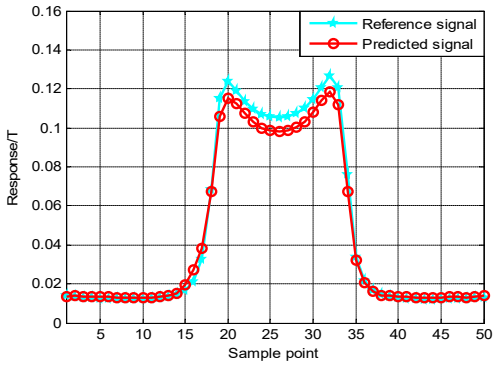

(b) The MFL single of MCS algorithm.

Figure 16. The result of MCS algorithm (sample No. 2).

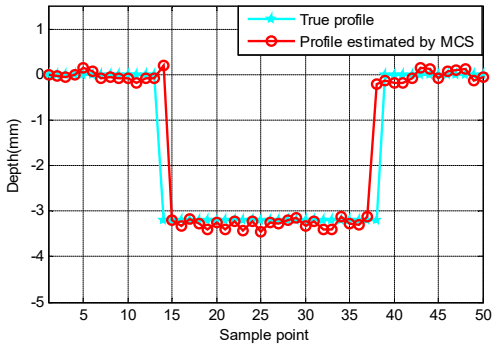

(a) The estimated defect profile of MCS algorithm.

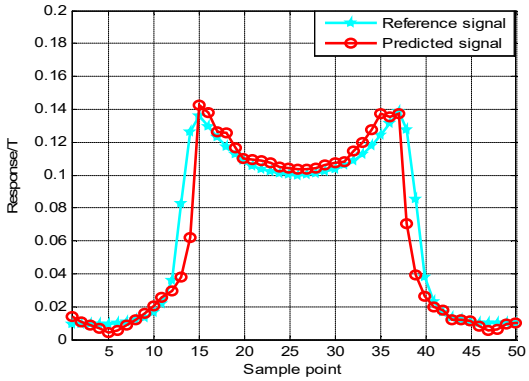

(b) The MFL single of MCS algorithm.

Figure 17. The result of MCS algorithm (sample No. 3).

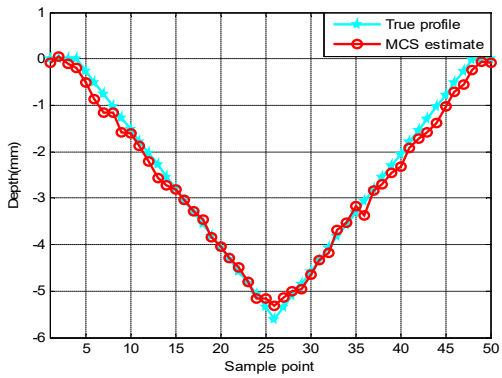

(a) The estimated defect profile of MCS algorithm.

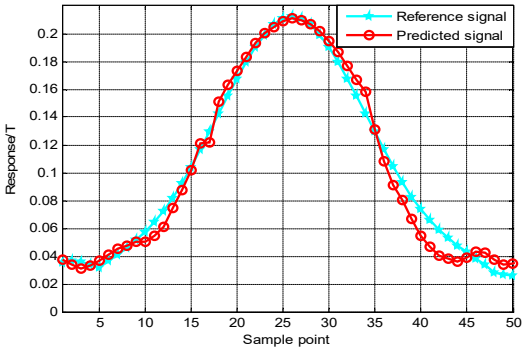

(b) The MFL single of MCS algorithm.

Figure 18. The result of MCS algorithm (sample No. 4).

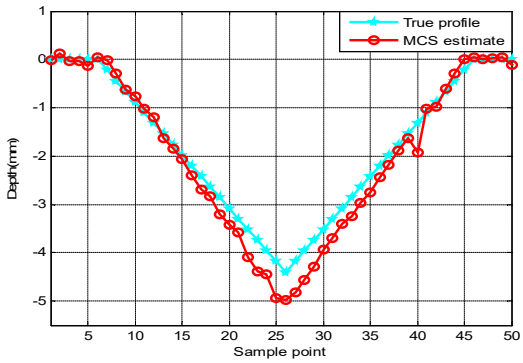

(a) The estimated defect profile of MCS algorithm.

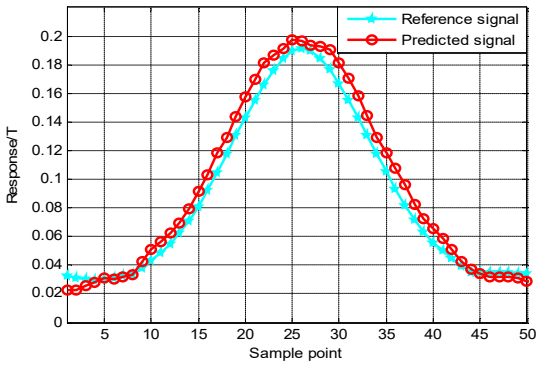

(b) The MFL single of MCS algorithm.

Figure 19. The result of MCS algorithm (sample No. 5).

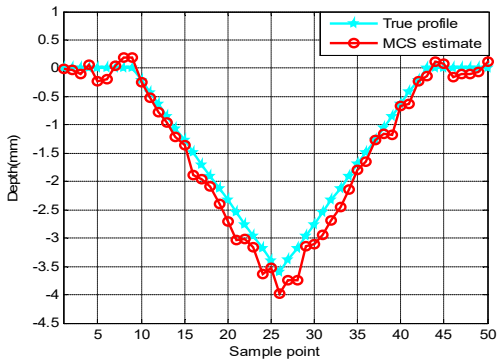

(a) The estimated defect profile of MCS algorithm.

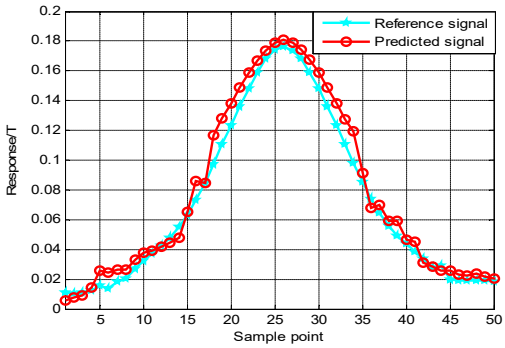

(b) The MFL single of MCS algorithm.

Figure 20. The result of MCS algorithm (sample No. 6).

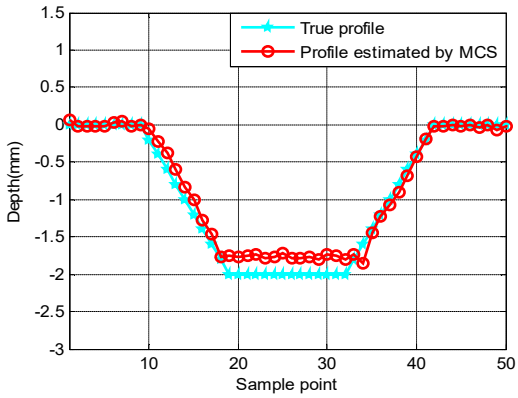

(a) The estimated defect profile of MCS algorithm.

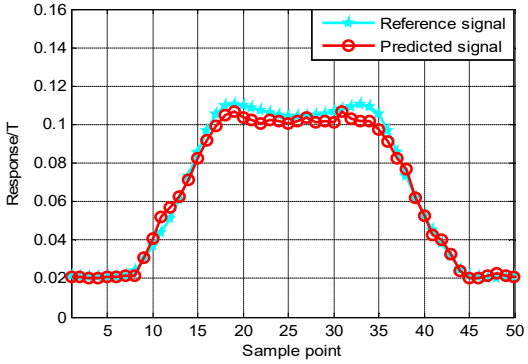

(b) The MFL single of MCS algorithm.

Figure 21. The result of MCS algorithm (sample No. 7).

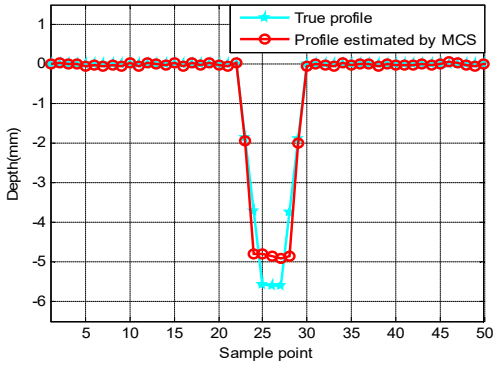

(a) The estimated defect profile of MCS algorithm.

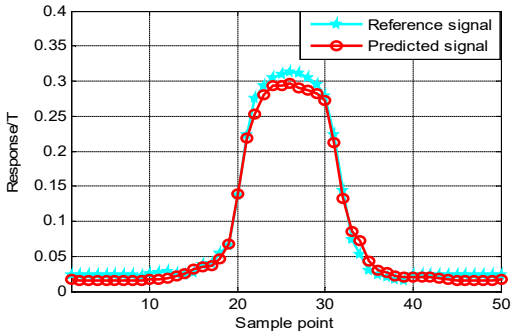

(b) The MFL single of MCS algorithm.

Figure 22. The result of MCS algorithm (sample No.8).

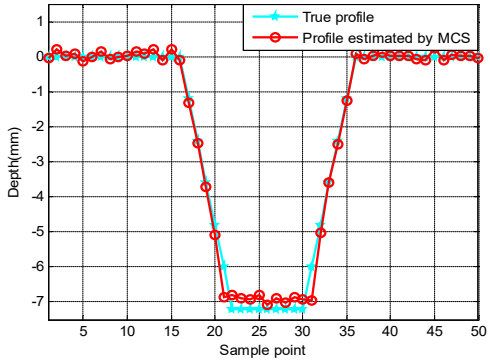

(a) The estimated defect profile of MCS algorithm.

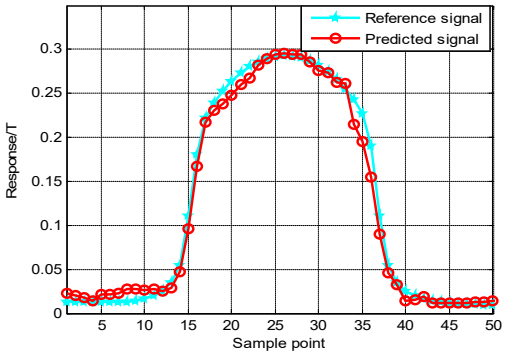

(b) The MFL single of MCS algorithm.

Figure 23. The result of MCS algorithm (sample No. 9).

Since the noise is added into the preference MFL signal, which causes some differences between the reference signal and the real value. Therefore, the accuracy of contour defect inversion will be affected by the noise and increases evaluation difficulty. From Table 5 and Figures 13 and 14, it is seen that the noise influences greatly the accuracy of the measurement. The PSD and PDE of the proposed approach were both higher than that case with no noise. The evaluated error increased due to the existence of the noise for the five algorithms. Among these algorithms, MCS and CS-PF had good robustness to noise. The change in PSD and PDE of PSO and DE, especially PSO, was larger than that of MCS and CS-PF.

Meanwhile, it is generally known that the predicted profiles achieved by MCS are clearly closer to the true profiles than CS-PF according to the average indicator PSD. It can be seen that the reconstructed profile of the proposed method can further improve the performance of CS-PF approach, which is a little better than CS-PF in the nine samples. The PSD and PDE of the proposed algorithm were lower than that of the other approaches. These results demonstrated that the proposed model was effective and efficient to reconstruct the defect profile in the presence of noise.

To further test the influence of the MCS on the accuracy of the inversion, an arbitrary defect was also used to reconstruct the profile. The number of the maximum iteration was 10,000. The predicted profile based on different methods is shown in Figure 24 and Table 6.

It is clearly seen that the accuracy of the predicted profile based on MCS is better than that of other four methods according to the PSD and PDE in Table 6. From Figure 24, it is also obvious that the predicted signal of MCS matches the reference signals accurately. Therefore, MCS algorithm is helpful for improving the profile reconstruction accuracy.

In addition, the experimental case was performed for testing the effectiveness of the MCS approach. The defect reconstruction based on MCS was applied to estimate real defect profile. As can be seen from the Figure 25, the MFL detector includes the three independent parts: the magnetic section, the record section and the battery section. The magnetic section was mainly used for detection. The record section was to save the data during the detection process. The main purpose of the battery section was to provide the required electric energy. The defect profile with known size was used to test the availability of the proposed algorithm. The results of the defect profile are plotted in Figure 26, the indicators of PSD and PDE are listed in Table 7. From Table 7, it can be seen that the method based on MCS is an effective method to construct the defect profile of the pipeline in the experimental case. The performance of MCS algorithm was superior to CS algorithm.

Table 6. The reconstruction results of different methods.

Method	PSD	PDE
CS	0.1409	1.1890
CS-PF	0.1219	1.1087
DE	0.1587	1.6738
PSO	0.2196	1.1525
MCS	**0.1006**	**0.6327**

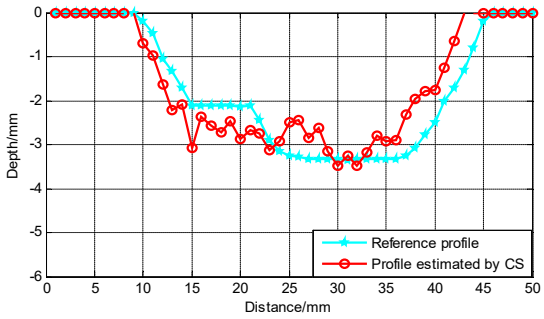

(a) Result of the inversion method based on CS.

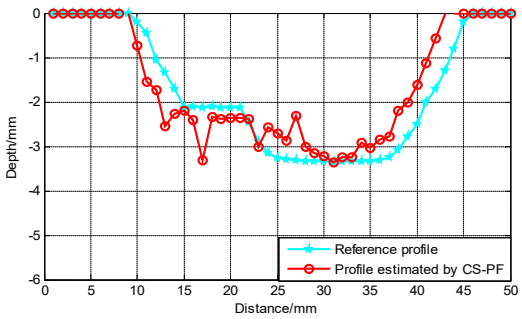

(b) Result of the inversion method based on CS-PF.

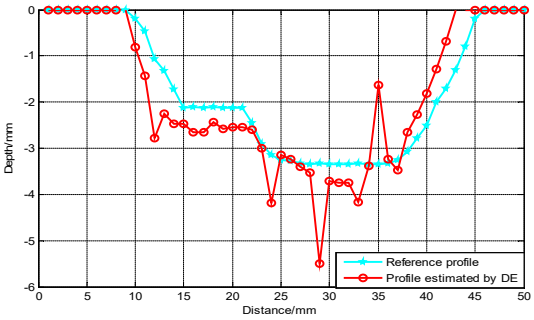

(c) Result of the inversion method based on DE.

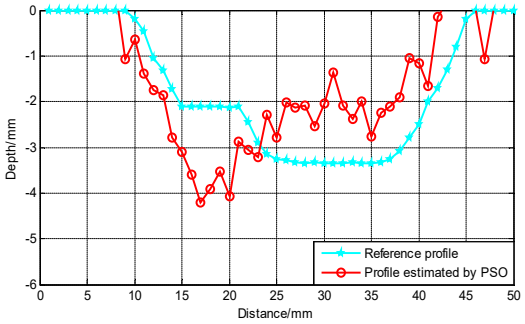

(d) Result of the inversion method based on PSO.

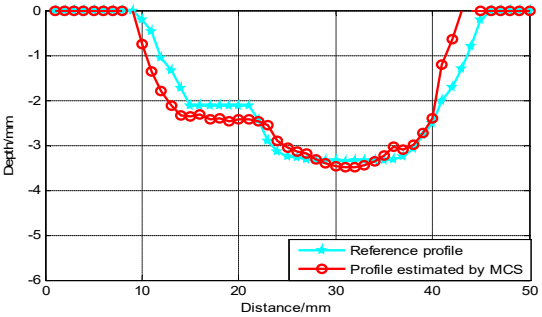

(e) Result of the inversion method based on MCS.

Figure 24. Inversion result of different methods.

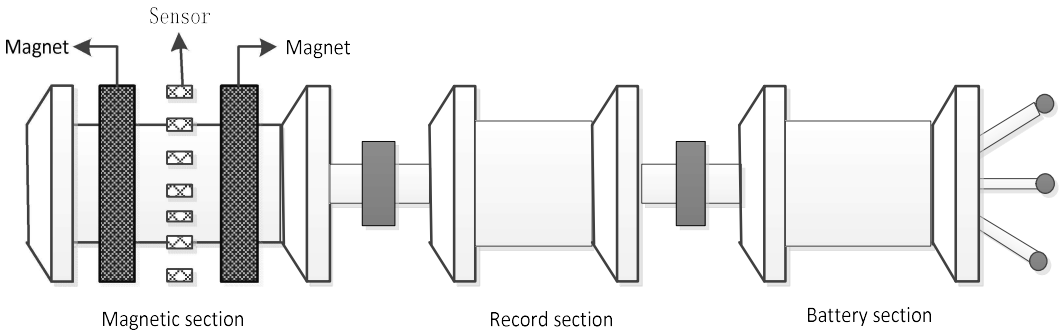

Figure 25. Structure drawing of experimental equipment.

Table 7. The reconstruction results of CS and proposed approach.

Sample index	PSD		PDE	
	CS	MCS	CS	MCS
Defect 1	0.157	0.051	1.388	0.656
Defect 2	0.121	0.056	1.172	0.589

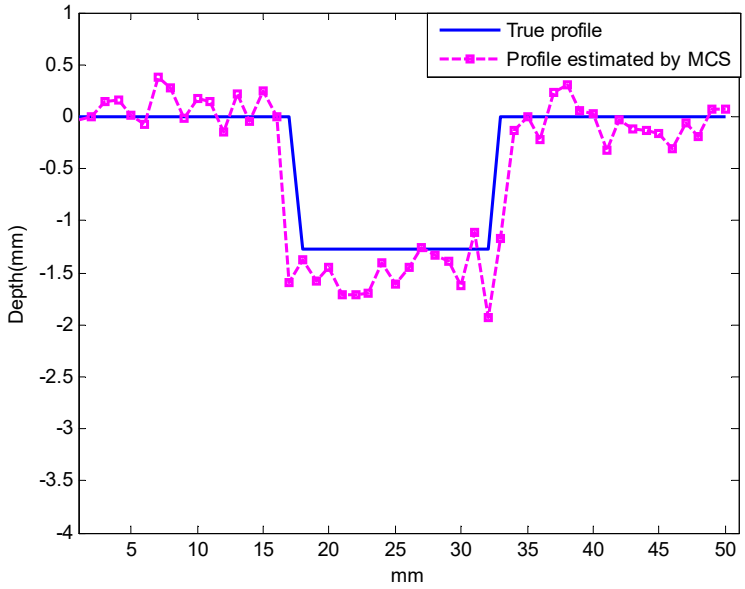

(a) Estimated profile for defect 1.

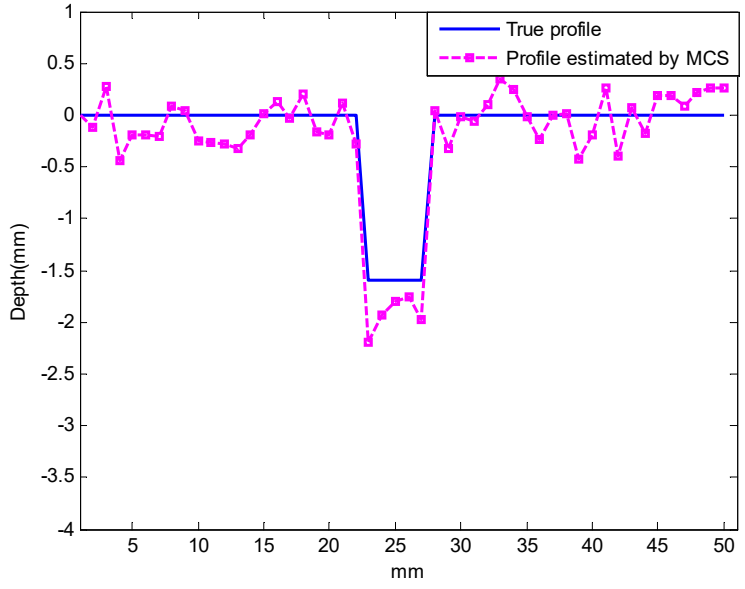

(b) Estimated profile for defect 2.

Figure 26. The result of the defect profile.

7. Conclusions

In this paper, we have proposed a novel defect profile reconstruction approach based on MCS. In the proposed approach, firstly, the MFL signal is employed as a key reference to estimate the quality of the predicted defect profiles in inversing process. Specifically, only the one-dimensional information with the largest error between the predicted signal and the reference signal is updated to reduce the interference caused by other dimension information. Secondly, to improve the diversity of the CS algorithm, multi-strategy DE optimization method is introduced to enrich the nest solution in rebuilt new nest process. Moreover, to optimize the structure of solution space, adaptive and dynamic settings of proportion parameter according to cost function or fitness function are discussed. The proposed MCS algorithm is tested by MFL experiment. In order to prove the ability of the reconstruction in noise circumstance, the proposed approach can reconstruct the defect profile by adding noise in preference MFL signal. The experiment results indicate that MCS can achieve higher accuracy. To reconstruct 3D defect profiles will be our future work with intelligent optimization methods.

Acknowledgements

This research was supported in part by the China Postdoctoral Science foundation (2020M680991) and in part by the Doctor Research Startup Foundation of Shenyang Aerospace University (18YB36).

Conflict of interest

All authors declare no conflicts of interest in this paper.

References

1. J. Wu, Y. Sun, Y. Kang, Y. Yang, Theoretical analyses of MFL signal affected by discontinuity orientation and sensor-scanning direction, *IEEE Trans. Magn.*, **51** (2015), 1–7.
2. J. Pavo, Numerical calculation method for pulsed eddy-current testing, *IEEE Trans. Mag.*, **38** (2002), 1169–1172.
3. B. Hartmut, P. Konstantin, M. Judith, Lorentz force eddy current testing: A novel NDE-technique, *Compel Int. J. Comput. Math. Electri. Electron. Eng.*, **33** (2013), 1965–1977.
4. Y. Shi, C. Zhang, R. Li, M. Cai, G. Jia, Theory and application of magnetic flux leakage pipeline detection, *Sensors*, **15** (2015), 31036–31055
5. E. G. Bazulin, A.V. Goncharsky, S. Y. Romanov, Inverse problems of ultrasonic tomography in nondestructive testing: mathematical methods and experiment, *Russ. J. Nondestr. Test.*, **55** (2019), 453–462.
6. W. Han, J. Xu, M. Zhou, M. Zhou, G. Tian, P. Wang, et al., Cuckoo search and particle filter-based inversing approach to estimating defects via magnetic flux leakage signals, *IEEE Trans. Magn.*, **52** (2016), 1–11.
7. Y. Li, G. Y. Tian, S. Ward, Numerical simulation on magnetic flux leakage evaluation at high speed, *NDT&E Int.*, **39** (2006), 367–373.

8. J. Chen, S. Huang, W. Zhao, Equivalent MFL model of pipelines for 3-D defect reconstruction using simulated annealing inversion procedure, *Int. J. Appl. Electromagn. Mech.*, **47** (2015), 551–561.
9. S. M. Dutta, F. H. Ghorbel, R. K. Stanley, Dipole modeling of magnetic flux leakage, *IEEE Trans. Magn.*, **45** (2009), 1959–1965.
10. P. Ramuhalli, L. Udpa, Electromagnetic NDE signal inversion by function-approximation neural network, *IEEE Trans. Magn.*, **38** (2002), 3633–3642.
11. R. H. Priewald, C. Magele, P. D. Ledger, N. R. Pearson, J. S. D. Mason, Fast magnetic flux leakage signal inversion for the reconstruction of arbitrary defect profiles in steel using finite elements, *IEEE Trans. Magn.*, **49** (2013), 506–516.
12. X. Song, S. Huang, W. Zhao, Quantitative interpretation for the magnetic flux leakage testing data based on neural network, *J. Wuhan Univ. Technol.*, **28** (2006), 443–447.
13. K. C. Hari, M. Nabi, S. V. Kulkarni, Improved FEM model for defect-shape construction from MFL signal by using genetic algorithm, *IET Sci. Meas. Technol.*, **1** (2007), 196–200.
14. E. Kurtulus, A. R. Yıldız, S. M. Sait, S. Bureerat, A novel hybrid Harris hawks- simulated annealing algorithm and RBF-based metamodel for design optimization of highway guardrails, *Materials Test.*, **62** (2020), 251–260.
15. F. M. Li, J. Feng, H. Zhang, J. Liu, S. Lu, D. Ma, Quick reconstruction of arbitrary pipeline defect profiles from MFL measurements employing modified harmony search algorithm, *IEEE Trans. Instrum. Meas.*, **67** (2018), 2200–2213.
16. Y. Zhang, Z. Ye, C. Wang, A fast method for rectangular crack sizes reconstruction in magnetic flux leakage testing, *NDT&E Int.*, **42** (2009), 369–375.
17. D. Dhiman, K. K. Singh, A. Slowik, V. Chang, A. R. Yildiz, A. Kaur, et al., EMoSOA: a new evolutionary multi-objective seagull optimization algorithm for global optimization, *Int. J. Mach. Learn. Cybern.*, **12** (2021), 571–596.
18. P. Champasak, N. Panagant, N. Pholdee, S. Bureerat, A. R. Yildiz, Self-adaptive many-objective meta-heuristic based on decomposition for many-objective conceptual design of a fixed wing unmanned aerial vehicle, *Aerosp. Sci. Technol.*, **100 (**2020), 105783.
19. B. S. Yıldız, A. R. Yıldız, E. I. Albak, H. Abderazek, S. M. Sait, S. Bureerat, Butterfly optimization algorithm for optimum shape design of automobile suspension components, *Materials Test.*, **62** (2020), 365–370.
20. W. Deng, J. Xu, H. Zhao, Y. Song, A novel gate resource allocation method using improved PSO-based QEA, *IEEE Trans. Intel. Transp. Syst.*, 2020.
21. Y. Song, D. Wu, W. Deng, X. Gao, T. Li, B. Zhang, et al, MPPCEDE: Multi-population parallel co-evolutionary differential evolution for parameter optimization, *Energy Convers. Manage.*, **228** (2021),113661.
22. W. Deng, J. Xu, Y. Song, H. Zhao, An effective improved co-evolution ant colony optimization algorithm with multi-strategies and its application, *Int. J. Bio-Inspired Comput.*, **16** (2020): 158–170.
23. M. A. E. Aziz, A. E. Hassanien, Modified cuckoo search algorithm with rough sets for feature selection, *Neural Comput. Appl.*, **29** (2018), 925–934.
24. Z. Cao, C. Lin, M. Zhou, R. Huang, Scheduling semiconductor testing facility by using Cuckoo search algorithm with reinforcement learning and surrogate modeling, *IEEE Trans. Autom. Eng.*, **16** (2019), 825–837.

25. I. Durgun, A. R. Yildiz, Structural design optimization of vehicle components using cuckoo search algorithm, *Materialprufung/Materials Test.*, **54** (2012), 185–188.
26. J. Ding, Q. Wang, Q. Zhang, Q. Ye, Y. Ma, A hybrid particle swarm optimization-cuckoo search algorithm and its engineering applications, *Math. Probl. Eng.*, **2019** (2019), 5213759.
27. A. M. Kamoona, J. C. Patra, A novel enhanced cuckoo search algorithm for contrast enhancement of gray scale images, *Appl. Soft Comput.*, **85** (2019), 105749.
28. W. Deng, J. J. Xu, Y. J. Song, H. M. Zhao, Differential evolution algorithm with wavelet basis function and optimal mutation strategy for complex optimization problem, *Appl. Soft Comput.*, **100** (2020), 106724.
29. J. Zhang, A. C. Sanderson, JADE: Adaptive differential evolution with optional external archive, *IEEE Trans. Evol. Comput.*, **13** (2009), 945–958.
30. T. Back., *Evolutionary Algorithms in Theory and Practice: Evolution Strategies, Evolutionary Programming, Genetic Algorithms*, Oxford University Press, Oxford, 1996.

AIMS Press